THE JOURNAL OF PHYSICAL CHEMISTRY C

ARTICLE

pubs.acs.org/JPCC

Picosecond Electron Injection Dynamics in Dye-Sensitized Oxides in the Presence of Electrolyte

Joep J. H. Pijpers,[†] Ronald Ulbricht,[†] Sofia Derossi,[‡] Joost N. H. Reek,[‡] and Mischa Bonn[†,*]

[†]FOM Institute for Atomic and Molecular Physics, Science Park 104, 1098 XG, Amsterdam, The Netherlands

[‡]University of Amsterdam (UvA), Supramolecular Catalysis, Science Park 904, 1098 XH Amsterdam, The Netherlands

Supporting Information

ABSTRACT: We employ time-resolved terahertz (THz) spectroscopy (TRTS) to directly monitor the picosecond dynamics of electron transfer in dye-sensitized oxides in the presence of an electrolyte phase. Understanding the time scale on which electrons are injected from the dye into the oxide phase in the presence of electrolyte is important for optimization of the solar cell efficiency. We quantify injection dynamics from two different dyes into both mesoporous TiO_2 and SnO_2 films. Measurements are performed in inert media (air, acetonitrile), in the presence of two different electrolytes (the conventional iodine/iodide couple and the recently reported disulfide/thiolate redox couple), and in the presence of two different electrolyte additives (Li^+ ions and *tert*-butyl pyridine). Electron injection dynamics in TiO_2 is found to occur on two time scales: sub-150 fs and ~10 ps, attributed to injection from the singlet and lower-lying triplet state, respectively. For SnO_2, injection is slower, despite the lower energy of the band edge. The slow injection observed for SnO_2 is attributed to the reduced density of electronic states in the material. We observe that for both oxides electron injection can be strongly retarded by changing the composition of the medium in which the sensitized oxide film is immersed. In particular, our results indicate that injection dynamics can be significantly slowed down in the presence of the disulfide/thiolate redox couple and/or *tert*-butyl pyridine.

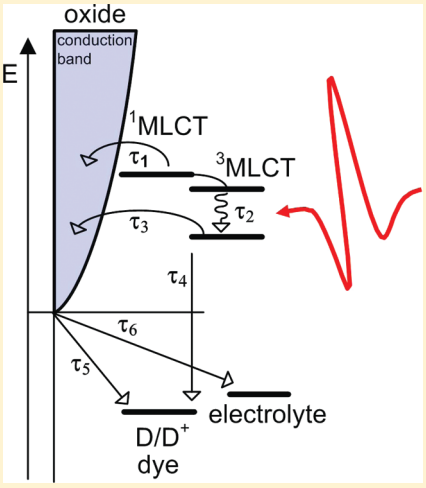

INTRODUCTION

The advance of dye-sensitized solar cells (DSCs) is a promising development in the quest for a technology that can provide cheap solar energy. The key building block of a DSC (or Grätzel cell) consists of a mesoporous oxide film that is sensitized with dye molecules that act as light absorbers.[1,2] Absorption of (sun)light brings the dyes into their excited state, and photoexcited charge carriers are extracted from the dyes by rapid electron transfer ("injection") into the electron-conducting mesoporous oxide film, which serves as the photoanode. The remaining positively charged dye molecules are reduced by a suitable redox couple in the electrolyte.

Previous studies have shown that the dynamics of electron injection from the adsorbed dye into TiO_2 occurs on an ultrafast (sub)picosecond time scale.[3−11] In all these experiments, the adsorbed dyes were excited with visible (femtosecond) pump pulses with wavelengths ranging from 400 to 630 nm. Initially,[3,6] the injection of electrons from excited dyes into oxides was monitored by probing the emergence of the spectral signature of the cationic dye (concurrently produced with injection) at near-infrared frequencies. More recently, probe light of mid-infrared[4,5,9] or terahertz (THz)[7,8,11] frequencies has been used to monitor the transient population of injected electrons in the oxide films directly. From the results of these research efforts, a model for the different dynamic processes that occur in a dye-sensitized oxide film after photoexcitation was constructed, which is summarized in Figure 1. The absorption of a visible photon by the dye molecule promotes an electron from the ground state (D) to the singlet excited state (^{1}MLCT). The population of electrons in the ^{1}MLCT state can decay via injection into TiO_2 (characterized by τ_1), but in parallel the ^{1}MLCT state can undergo intersystem crossing to the excited manifold of the triplet ^{3}MLCT state, followed by intramolecular vibrational relaxation to the ^{3}MLCT ground state (characterized by τ_2). Significant injection from the singlet state into TiO_2 occurs only when τ_1 is small compared to τ_2. Reversely, in the situation where $\tau_1 > \tau_2$, the majority of the excited molecules in the ^{1}MLCT state will decay to the ^{3}MLCT state. From the ^{3}MLCT state, electrons can either be injected into TiO_2 or recombine to the ground state (characterized by time scales τ_3 and τ_4, respectively). Once injected into the oxide, the electrons will thermalize rapidly to the TiO_2 conduction band edge, from which they can recombine with the adsorbed cationic dye molecule (D^+) or with the redox couple in the electrolyte (characterized by time scales τ_5 and τ_6, respectively).

Received: November 1, 2010
Revised: December 23, 2010
Published: January 11, 2011

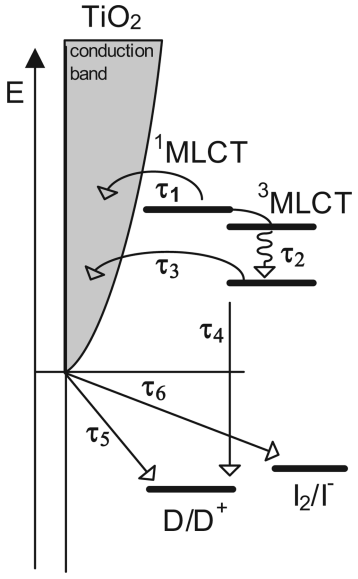

Figure 1. Schematic diagram of the energy levels in a dye molecule with respect to the conduction band of the TiO_2 to which the dye is adsorbed. All possible dynamic processes after photoexcitation of the dye (indicated by arrows) are explained in the text.

The theory generally used to predict the rate of electron transfer between two chemical species was developed in the 1960s by Marcus,[12] among others. As discussed in ref 4, this theory can be adapted to describe electron transfer between dyes and bulk semiconducting oxides. The three parameters that govern the rate of electron injection are electronic coupling between the electron-donating orbital of the adsorbed dye and the electron-accepting orbitals of the semiconductor, the density of states (DOS) in the conduction band of the electron-accepting semiconductor, and the free energy difference between the dye-excited state and the conduction band edge of the oxide.[4] The dependence of the dye-semiconductor electron transfer rate on these parameters for the case of weak coupling (nonadiabatic limit) is given by the following expression[4,5]

$$K_{ET} = \frac{2\pi}{h}\int_{-\infty}^{\infty} dE\rho(E)|H(E)|^2 \frac{1}{\sqrt{4\pi\lambda k_b T}} \exp\left[-\frac{(\lambda+\Delta G_0 - E)^2}{4\lambda k_b T}\right] \quad (1)$$

In this equation, ΔG_0 is the energy difference between the conduction band edge and the redox potential of the dye excited state; $\rho(E)$ is the density of semiconductor states at energy E from the conduction band edge; $H(E)$ is the average electronic coupling between the excited dye state and the different states in the semiconductor at energy E; and λ is the reorganization energy. Equation 1 clearly illustrates that the injection rate increases for higher density of acceptor states, stronger electronic coupling, and a larger free energy difference ΔG_0. Indeed, experimental reports show that injection from the dye singlet state into TiO_2 is faster than injection from the dye triplet state:[4−6,13] this observation has been explained by the larger density of accepting states at the (higher) energy of the ^{1}MLCT state.[5] The effect of electronic coupling has been investigated by introducing a varying number of CH_2 units between the carboxylate linking group and the electron-donating bipyridine ligand. For increasing distance between the electron-donating ligand and the electron-accepting TiO_2 (less electronic coupling), the rate of electron injection has been demonstrated to drop considerably.[4] Finally, the expected influence of ΔG_0 on injection dynamics was confirmed by a systematic study of a series of dyes with different excited state potentials (but comparable electronic coupling properties).[4]

In all the previously mentioned transient absorption studies, the dye-sensitized oxide films were measured in inert solvents (e.g., ethylene carbonate, air, acetonitrile, etc.) without the electrolyte components being present. When measured in real electrolyte solutions, electron injection dynamics has been shown to be considerably slower.[13,14] At first sight, one might be tempted to conclude that slow injection exacerbates device performance of a DSC since slower charge separation potentially leads to increased recombination of excited dyes to the ground state. However, it is known that the addition of 4-*tert*-butyl pyridine (TBP) to the electrolyte solution significantly benefits the solar cell operation by increasing the V_{oc}, in spite of orders of magnitude slower injection dynamics.[13,14] This seeming contradiction has been explained by the concept of "kinetic redundancy":[13,14] first, electron injection on a subpicosecond time scale is not required for efficient charge separation since the lifetime of the excited dye is on the order of ~50 ns,[13] indicating that the system is "kinetically redundant". Second, a kinetically redundant DSC is suboptimal since ultrafast electron injection is associated with a low energetic value of the TiO_2 conduction band edge relative to energy level of the electron-donating excited dye molecule. The disadvantage of positioning the TiO_2 conduction band edge at low energy values is that the conduction band edge moves toward the Fermi level, as a result of which the occupancy of trapped states and conduction states increases.[15] This is important since recombination of electrons in TiO_2 with the cationic dye or the redox couple has been shown to depend strongly on the occupancy of trap and conduction states.[15] Summarizing, (sub)picosecond electron injection from dyes into TiO_2 is much faster than required for efficient charge separation and is also accompanied by increased recombination: hence, ultrafast injection does not automatically lead to higher solar cell efficiency.

From the above, it is evident that understanding and control of the dye-oxide electron injection dynamics are desirable for optimization of DSC performance. In this article, we employ time-resolved THz spectroscopy (TRTS) to compare the effect of two active electrolyte species, i.e., the conventional iodine/iodide-based redox couple (I_3^-/I^-) and a recently developed disulfide/thiolate redox (T_2/T^-) couple.[16] Advantages of the latter redox couple include low absorption of visible light and reduced corrosion of metallic contacts, making this recently introduced redox couple promising for commercial DSCs.[16] Also, we investigate the effect of the electrolyte additives (Li^+-ions and TBP) and the oxide material (TiO_2 and SnO_2) on electron injection dynamics. Our results indicate that injection dynamics is significantly influenced by the electrolyte species and electrolyte additives, demonstrating that judicious choice of the electrolyte composition may lead to better DSC performance.

EXPERIMENTAL PROCEDURES

Sample Preparation. Mesoporous TiO_2 and SnO_2 films were prepared by spreading out viscous dispersions of colloidal TiO_2 and SnO_2 particles on a microscope slide. For the TiO_2 film, an ethanol-based paste containing 15 nm TiO_2 particles was

purchased from Solaronix (T-LALT). A SnO_2 paste was obtained by dispersing SnO_2 powder (Aldrich, average particle size <100 nm) in an ethanol solution containing NH_4OH (added to stabilize the colloidal suspension of SnO_2 particles). After deposition of the paste, the films were dried at 115 °C for 30 min and subsequently annealed in air at 450 °C for 2 h. Sensitization was achieved by immersing the oxide films (stored at 90 °C to remove the hydroxyl groups terminating the oxide surface) in a 0.1 mM dye solution (either N3 or N719 dye, both obtained from Solaronix) in anhydrous methanol for several hours. The absorption spectra of TiO_2 films sensitized with N3 and N719 are given in the Supporting Information.

Injection dynamics was studied for two different electrolyte redox couples. First, we use an I_3^-/I^- redox couple dissolved in acetonitrile as electrolyte, which is commonly used in Grätzel solar cells. Second, the redox couple T_2/T^- was synthesized following ref 16, where T^- represents the 5-mercapto-1-methyltetrazole ion and T_2 stands for its charge-neutral dimer. The NMR spectra of the synthesized compounds were in good agreement with literature reports.[16] In contrast to the I_3^-/I^- couple, the T_2/T^- system absorbs little visible light (see Supporting Information). To study the effect of electrolyte additives, we investigated electron injection dynamics in I_3^-/I^- electrolytes with lithium ions and/or 4-*tert*-butyl pyridine (TBP) added. To account for the effect of the various electrolyte components on injection dynamics, we investigated a number of electrolyte compositions, following ref 13:

- Electrolyte A: 0.6 M tetrabutylammonium iodide (TBA-I), 0.1 M lithium iodide, 0.5 M TBP, and 0.1 M iodine dissolved in acetonitrile.
- Electrolyte B: similar to electrolyte A, but without the LiI.
- Electrolyte C: similar to electrolyte A, but without TBP

All chemicals were electrochemical or HPLC grade and were purchased from Fluka.

Time-Resolved Terahertz Spectroscopy. We employed TRTS[17] to assess the time scale of electron injection from photoexcited dye molecules into the oxide. In a typical pump−probe experiment, we excite the sample with 590 nm pulses (~100 fs) and monitor the carrier population in the oxide with a probe of THz frequencies. This probe beam contains frequency components from 0.2 to 2 THz.[17] A frequency of 1 THz corresponds to a photon energy of 4 meV, which is well below the electronic transitions of bulk semiconductors and the resonances in the dye molecules. Rather than interacting resonantly with electronic or vibrational transitions in the system, the oscillating electric field of the THz probe interacts strongly with free charge carriers. The interaction of THz light with free carriers in semiconductors is usually described by the Drude model. In this model, the absorption of THz light by free carriers is described by the real part of the complex conductivity,[11,17,18] which corresponds to the dissipative (imaginary) part of the response function (or dielectric function). The resonance for absorption of electromagnetic light by free carriers (peak of the real conductivity) is positioned at $\omega = 0$. In many types of harmonic motion, like vibrations and rotations of molecules, the resonance is positioned at $\omega > 0$. The position of the resonance is determined by the restoring force, whose force constant is the proportionality factor between the displacement of the particle and this force. For free carriers, the force constant is zero, giving rise to a linear damping of the electronic motion and explaining why the resonance in the Drude model is positioned at $\omega = 0$. The real conductivity provides direct information about the number and mobility of free carriers in semiconductors. As such, TRTS has been widely used to probe the carrier dynamics in bulk semiconductors[19,20] and mesoporous semiconducting oxides.[21−23] In the case of dye-sensitized mesoporous oxide films, the pump pulse will selectively excite the dye molecules, and injection of electrons is reflected by the increase of ΔE_{THz} as a function of pump−probe delay. Previously, TRTS measurements have been performed on dye-sensitized TiO_2 films in inert solvents, indicating (sub)picosecond injection dynamics.[7,8,10,11] We extend these studies to dye-sensitized films immersed in an electrolyte solution. To be able to do so, the path length of the electrolyte phase should be short since THz light is strongly absorbed by both the electrolytes and the polar solvents (like acetonitrile) that are commonly used for electrolyte solutions. For this reason, the microscope slide on which the oxide film was deposited was covered with a second microscope slide, and subsequently, the oxide matrix between the two microscope slides was interpenetrated with the electrolyte solution using capillary forces, resulting in a very thin electrolyte phase in the sample. We estimate that the thickness of the electrolyte phase amounted to ~10 μm, which was thin enough to have considerable transmission of THz light. This estimation was done by comparing the transmission of THz light through the electrolyte phase in our samples with the transmission of THz light through cuvets of known thickness (0.1 and 0.5 mm) containing acetonitrile. The thickness of the electrolyte phase was then obtained by extrapolation. After addition of electrolyte A, the absorption band of the dye-sensitized film at 535 nm shifted slightly to shorter wavelengths, as can be seen in the inset of Figure S1(b) (Supporting Information).

DSC Devices. Complete DSCs were constructed by preparing functionalized oxide films (similar procedure as above) on a conducting ITO substrate (1 × 1 cm) instead of using microscope slides. The dye-sensitized oxide electrode and a Pt-coated counter-electrode were sandwiched in an open cell configuration. The electrolyte was an acetonitrile-based solution containing I^-/I_2 (0.7 M TBA-I, 0.1 M I_2) or T^-/T_2 (0.4 M T^-, 0.4 M T_2) as the redox couple. Current−voltage measurements were performed in a solar simulator (Wacom) using a 5 kW Xe-lamp (type WXS-300S-50, AM1.5G).

RESULTS AND DISCUSSION

Figure 2 shows the THz modulation for TiO_2 films sensitized with N719- and N3-dye that were immersed in acetonitrile. The THz signal represents the population of injected electrons in TiO_2. The data in Figure 2 were obtained after exciting the films with 2 $\mu J/mm^2$ 590 nm pulses. We verified that the amplitude of the THz signal scaled with the excitation intensity and that its shape (i.e., the time-evolution) remained the same for lower excitation fluences. Also, we checked that the high excitation fluence did not cause any photocorrosion, by verifying that the amplitude and the shape of the THz signal remained the same during ~1 h of data acquisition. When the sensitized films were measured in air, however, the amplitude of the THz signal strongly decreased as a function of time. This observed photodegradation has been explained previously by oxygen-induced desulfurization of the thiocyanide (SCN) ligands.[3]

The data in Figure 2 exhibit a fast rise of the THz signal, followed by an additional ingrowth of the signal on a longer time scale. This "biphasic" injection kinetics is typical for TiO_2 sensitized with ruthenium-based dyes.[3−6,11,13] The fast component

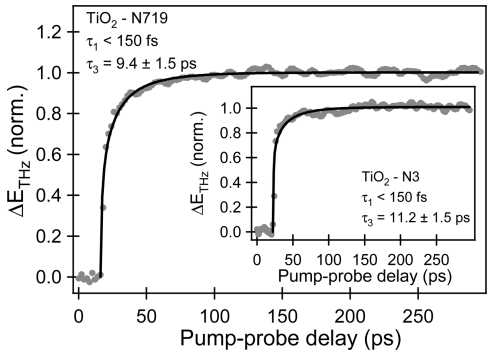

Figure 2. THz modulation—proportional to the product of electron density and mobility—for nanostructured TiO_2 films sensitized with N719 and N3 (inset), immersed in acetonitrile. The films were excited with 2 $\mu J/mm^2$ pulses, with a duration of 100 fs and centered at 590 nm. The data can be described with biphasic injection kinetics (solid lines), as explained in the text, with time constants indicated in the graph.

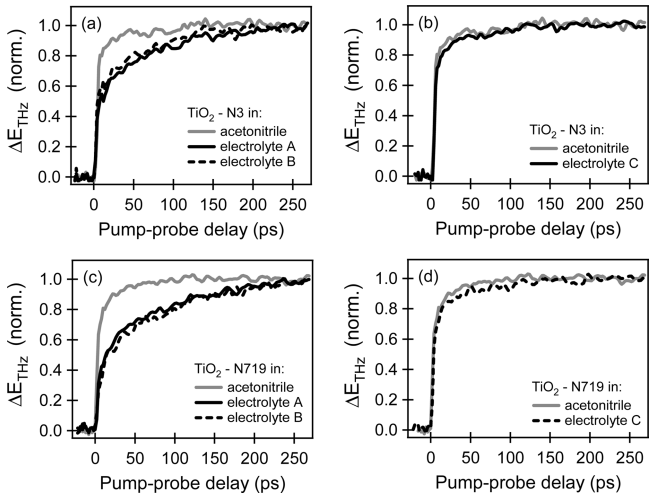

Figure 3. THz modulation—proportional to the product of electron density and mobility—for TiO_2—N3 (a + b) and TiO_2—N719 (c + d) in different electrolytes. The composition of electrolytes A, B, and C is given in the Experimental Section.

has been attributed to injection from the ^{1}MLCT state (characterized by τ_1 in Figure 1), and the slower component has been assigned to injection from the ^{3}MLCT state (characterized by τ_3).[5] Injection from the high-energy singlet state is only possible if it occurs on time scales faster than, or comparable to, intersystem crossing from the singlet to the triplet state (characterized by τ_2 in Figure 1). In the literature, ultrafast injection from the singlet state in N3—TiO_2 has indeed been reported to occur with a time constant of ~25—50 fs,[24] while intersystem crossing from the singlet to the triplet state was found to occur within 30 or 75 fs (for TiO_2—N3 in air and ethanol, respectively).[25] The fast injection from the singlet state in Ru—TiO_2 systems can be explained by the very high electron effective mass in TiO_2 (~10·m_e),[26] resulting in an very high DOS in the TiO_2 conduction band. Additionally, the conduction band of TiO_2 is formed from empty 3d orbitals of Ti^{4+} ions, having π symmetry.[4] Since the electron-donating orbital of the dye is the π^* orbital of the bipyridine ligand, there is strong overlap between the donating and accepting orbitals, resulting in strong electronic coupling. For the case of biphasic injection, the amplitude of the fast component is determined by the ratio of τ_1 and τ_2.

The data in Figure 2 can be described very well with the following equation[5]

$$N_e = A(1 - \exp(-t/\tau_1)) + B(1 - \exp(-t/\tau_3)^{\alpha}) \quad (2)$$

In this equation, N_e corresponds to the population of injected electrons; A and B are the amplitudes of injection from the singlet and triplet state, respectively; and α is the so-called stretch parameter. The use of the latter parameter is required since electron injection is not monoexponential because of local inhomogeneities in the sensitized film (leading to local shifts of the conduction band edge, electronic coupling, etc.).[5,6,14] For the relatively slow triplet injection, the time resolution of our THz experiment is good enough to clearly resolve injection dynamics, and we describe the multiexponential nature of the triplet injection component by a stretched exponential, characterized by the stretch parameter α.[5,6,14] For α = 1, the equation reduces to simple exponential kinetics. For the fast singlet injection, we have insufficient temporal resolution to resolve such potential inhomogeneities, and the stretched exponential is not considered. Fitting the data in Figure 2 to eq 2 yields values for τ_3 of 11.2 ± 1.5 ps for TiO_2—N3 and 9.4 ± 1.5 ps for TiO_2—N719. For both samples, the value of α was fixed to 0.7: this value resulted in much better fits than for α = 1. Since the heterogeneity of the samples (and hence of the injection process) is not expected to vary much in the different experiments, we decided to fix this parameter in subsequent fits. An upper limit for the time constant τ_1 of 150 fs was obtained for both samples, which was limited by the instrument response function of the TRTS setup.

In a complete DSC, the dye-sensitized film is typically immersed in an iodine/iodide (I_3^-/I^-) acetonitrile solution containing different additives (Li^+-ions and TBP) that optimize solar cell performance. In such complete solar cells, a significant retardation of injection dynamics has been observed previously.[13,14] In these studies, injection dynamics was determined using transient absorption and emission measurements, in which potential deactivation processes other than injection were corrected for by control measurements on dye-sensitized ZrO_2 films, in which electron injection is energetically not allowed. Although these control experiments have proven very valuable in determining the electron injection dynamics in dye—TiO_2 systems, it can never be guaranteed that the surface chemistry (e.g., dye cluster formation) of a dye—ZrO_2 interface is exactly the same as that of a dye—TiO_2 interface. Therefore, we did complementary THz experiments on dye-sensitized TiO_2 films immersed in I_3^-/I^- electrolyte solutions with composition similar to those in refs 13 and 14 to directly probe the emergence of electrons in TiO_2.

The THz data for various electrolyte surroundings (see Experimental Section for precise compositions) are presented in Figure 3. When the films were immersed in electrolyte A (both Li^+ ions and TBP added) or in electrolyte B (only TBP added), the amplitude of the fast component of the biphasic kinetics in Figure 3 is reduced markedly. However, when immersing the samples in electrolyte C (only Li^+ ions added), the injection dynamics was comparable to the dynamics observed for films immersed in (inert) acetonitrile. These observations are in agreement with previous transient absorption and emission measurements.[13,14] In the presence of electrolyte A, the value of τ_3 (obtained from fitting the data in Figure 3) was found to be 50 ± 10 ps for TiO_2—N3 and 60 ± 10 ps for TiO_2—N719 for α = 0.7. Since the injection is not fully completed at the longest detected

delay time, τ = 300 ps, the error in the extracted time constants is larger than in Figure 2, but the data in Figure 3 clearly show that the injection dynamics is strongly retarded in the presence of electrolyte A and B, compared to immersion in acetonitrile or electrolyte C where the majority of electrons is injected within approximately tens of picoseconds. The results in Figure 3 are fully consistent with previous reports on the effect of electrolyte composition on injection dynamics.[13,14] The authors in these reports have argued that the slower injection dynamics can be explained by the influence of the electrolyte additives (i.e., TBP and Li^+ ions) on the energetics of the TiO_2 conduction band. Briefly, spectro-electrochemical studies have indicated that the presence of TBP in the electrolyte leads to shifts of the TiO_2 conduction band to higher energies.[15] Similar studies have revealed that addition of Li^+ ions has the opposite effect: for increasing Li^+ concentration, the conduction band of TiO_2 shifts to lower energies. These shifts in the position of the conduction band cause variations in the density of TiO_2-accepting states relative to the singlet and triplet dye excited state. For the Li^+ and TBP concentrations used in this study, the induced shift of the conduction band can be as high as 300 meV,[13,15] resulting in a 20-fold decrease or increase of the number of accepting TiO_2 states.[13] Hence, the addition of Li^+ (electrolyte C) facilitates fast electron injection, which is also corroborated by the presence of a fast injection component in Figure 3(b) and (d). The fact that there is still a dispersive slow injection component in the presence of electrolyte C can be attributed to local variations of the Li^+ concentration in the homogeneous film.[13,14] Addition of TBP to the electrolyte strongly retards the injection dynamics, even in the case where Li^+ ions are present (electrolyte B). Presumably, since TBP and Li^+ ions shift the band edge in opposite directions, the addition of 0.1 M Li^+ does not fully compensate the upward shift induced by the TBP. In Figure 3(a) and (c), it can be seen that the fast injection component decreases in the presence of electrolytes A and B. This observation can also be explained by the reduction of the density of accepting states at the position of the ^{1}MLCT level, slowing down ultrafast injection from dye molecules in the ^{1}MLCT state. Hence, intersystem crossing from the ^{1}MLCT to the ^{3}MLCT state (characterized by τ_2 in Figure 1) is likely to become the dominating decay pathway for excited dye molecules in the singlet state, as was also argued in ref 14. Future studies will be carried out to determine if the fast injection disappears completely upon increasing the TBP concentration.

To further investigate the effect of the parameters determining electron transfer rates (density of accepting states in the oxide, electronic coupling, and the magnitude of ΔG_0), we studied electron injection dynamics in N3-sensitized SnO_2 films. Although the SnO_2 particle size (<100 nm) was somewhat larger than the TiO_2 particle size (15 nm), the morphologies of the sintered films (as determined by SEM imaging) and the specific surface area (as determined by N_2 adsorption) were very similar. Furthermore, we have performed measurements as a function of TiO_2 particle size in the 10−50 nm range, and these different particles do not display a marked dependence of the injection dynamics on that size. Therefore, we do not expect that the larger SnO_2 particle size has a significant effect on the injection dynamics. Figure 4 shows a comparison of the THz modulation for N3-sensitized SnO_2 and TiO_2 films. Although the energy of the SnO_2 conducting band edge is roughly 0.5 eV lower than the TiO_2 conduction band edge,[2,27] electron injection into SnO_2 is slower compared to injection into TiO_2. This observation can be

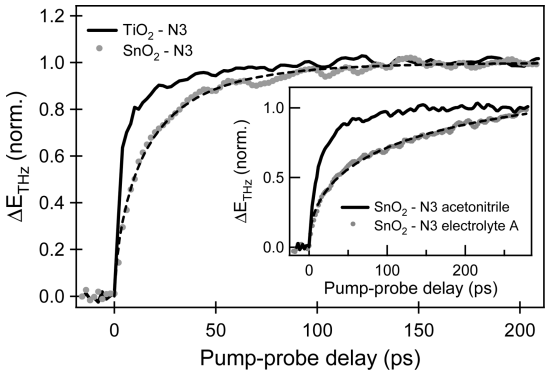

Figure 4. THz modulation—proportional to the product of electron density and mobility—for N3-sensitized SnO_2 (gray dots) and TiO_2 (continuous black lines) following excitation with 590 nm pulses. In contrast with injection into TiO_2, electron injection into SnO_2 is not biphasic and can be fit with a stretched exponential ingrowth (dashed black line). The dynamics of the THz data is attributed to injection from the ^{3}MLCT state, as explained in the text. The inset shows a comparison of injection dynamics into SnO_2 in acetonitrile and electrolyte A.

explained by the considerably lower electron effective mass in SnO_2 ($\sim 0.28 \cdot m_e$),[28] leading to a much lower DOS in the SnO_2 conduction band,[4,5,9] as follows from the nearly free electron model.[29] Furthermore, the conduction band of SnO_2 is formed by empty 5s orbitals of the Sn^{4+} ions. As a result, the overlap between the electron-donating π^* orbitals of the bipyridine ligands and the electron-accepting orbitals in the SnO_2 conduction band is not optimal, and electronic coupling is relatively weak.[4] Apparently for this system, DOS and electronic coupling arguments have a more pronounced influence on injection kinetics than the potential difference between the excited state dye and the conduction band edge. The data in Figure 4 can be fit with a single stretched exponential ingrowth ($N_e = B(1 - \exp(-t/\tau 3)^{\alpha})$, fits represented by the dashed black line in Figure 4. This indicates that the kinetics of electron injection into SnO_2 is not biphasic, in contrast to injection in the dye−TiO_2 system. The fit yields a time constant associated with electron injection of ∼16 ± 1 ps for α = 0.7. We attribute this kinetics to injection from the ^{3}MLCT state since the singlet state lifetime is not expected to increase by orders of magnitude upon interacting with SnO_2. The absence of biphasic injection kinetics in the dye−SnO_2 system indicates that injection from the ^{1}MLCT state is no longer fast enough to compete with relaxation to the ^{3}MLCT state ($\tau_1 \gg \tau_2$).

The inset of Figure 4 shows a comparison of injection dynamics of the N3-sensitized SnO_2 immersed in acetonitrile (black solid line) and electrolyte A (gray dots). Clearly, electron injection in the presence of electrolyte A slows down significantly also for SnO_2. Analogous to the dye−TiO_2 system immersed in electrolyte A, this retardation of electron injection is likely caused by a positive shift of the SnO_2 conduction band edge, leading to reduced DOS of electron-accepting energy levels in SnO_2. The data in the inset of Figure 4 are fit with the stretched exponential function yielding a time constant of electron injection of ∼160 ± 20 ps. The data in Figure 4 indicate that the presence of electrolyte A reduces the rate of electron injection by at least 1 order of magnitude, which is in agreement with ref 13. The similar trend observed for dye−TiO_2 and dye−SnO_2 when immersing the films in electrolyte indicates that the main effect of the electrolyte (shifting of the oxide conduction band edge, leading to changes of the DOS in the oxide at the position of the ^{1}MLCT

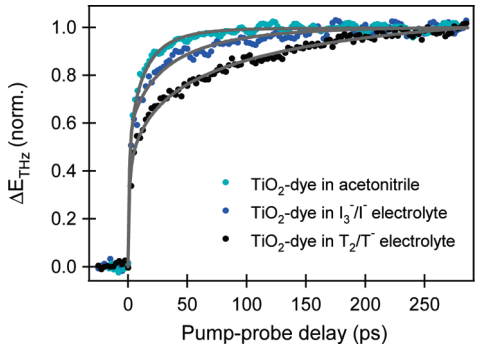

Figure 5. THz modulation—proportional to the product of electron density and mobility—for nanostructured TiO_2 films sensitized with N719, immersed in acetonitrile (light blue dots), I_3^-/I^- in acetonitrile (blue dots, 0.7 M TBA I and 0.1 M I_2), and T_2/T^- in acetonitrile (black dots, 0.4 M T_2 and 0.1 M T^-). Note the slow-down of injection in the T_2/T^- electrolyte.

and ^{3}MLCT states), can likely be generalized to other dye−oxide systems.

As illustrated above, it becomes apparent that electrolyte additives and the oxide material can significantly influence electron injection dynamics. The electrolyte couple itself is another potential candidate for influencing these injection dynamics. From time-resolved emission studies,[14] it was found that the presence of the I_3^-/I^- couple alone does not result in significant changes of electron injection dynamics. Since the time resolution of this technique was ∼60 ps, we did TRTS measurements (∼150 fs time resolution) to confirm these findings for shorter time scales. Furthermore, we investigated the effect of the presence of the T_2/T^- redox couple on injection dynamics. Figure 5 shows a comparison of TRTS measurements on TiO_2−dye samples immersed in acetonitrile (light blue) and in I_3^-/I^- in acetonitrile (dark blue dots). Fitting the data in Figure 5 with eq 2, we find a retardation of injection dynamics from 9.4 ± 1.5 ps in acetonitrile to 29 ± 2.0 ps for the iodide solution. It is conceivable that the retardation caused by the presence of the I_3^-/I^- couple does not lead to significant changes for the electron injection efficiency, as was also concluded in ref 14, since the lifetime of the excited dye is ∼50 ns. Interestingly, the injection dynamics is slowed down further in the presence of the T_2/T^- redox couple, as shown in Figure 5 (black dots). Clearly, the electron injection is significantly retarded and is not completed at a pump−probe delay of 300 ps. While the slow injection dynamics makes it challenging to extract an *exact* value for the time constant of electron injection, the curvature of the signal allows for a reasonably accurate estimate of the injection time constant of 65 ± 20 ps. A possible explanation for this retardation of injection dynamics is that the presence of T_2/T^- species influences the interfacial charge densities/dipoles, resulting in the "potential-determining" behavior similar toTBP.

We attempted to correlate the different injection dynamics of the two redox couples to solar cell performance. For this purpose, we measured the *IV* characteristics of three solar cells based on the T_2/T^- couple and three solar cells based on the I_3^-/I^- couple. Figure 6 shows typical *IV* curves for these solar cells. For both the T_2/T^- and the I_3^-/I^- couple, the average V_{oc} was ∼0.59 V, and the I_{sc} of the cells varied from 5 to 7 mA/cm^2. Since the cells were measured in open cell configuration, the fill factors were rather low (∼0.3−0.4), as can be seen in Figure 6. In ref 13, a correlation was found between slow injection dynamics and an

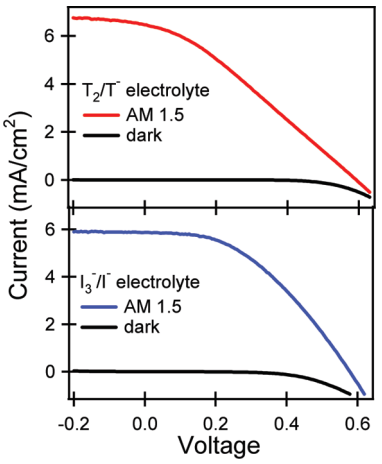

Figure 6. Typical $I-V$ curves for solar cells based on TiO_2−N3 anodes in T_2/T^- electrolyte (red line) and I_3^-/I^- electrolyte (blue line) under AM1.5G illumination. The black lines are the corresponding dark *IV* curves.

increased V_{oc}, which was attributed to shifts of the TiO_2 conduction band edge. We did not observe higher V_{oc} values for T_2/T^- based solar cells, in spite of the slower injection kinetics (see Figure 5). Hence, the IV curves in Figure 6 do not provide further evidence of TiO_2 conduction band shifts. A possible explanation for our inability to draw conclusions about the band shift from V_{oc}, however, is that the V_{oc} is not only determined by the conduction band position but also by the injection rate, regeneration rate, and recombination rates (to electrolyte species and oxidized dye). The observation that the values of I_{sc} are similar for the T_2/T^- and the I_3^-/I^- redox couples suggests that the slower injection in the presence of T_2/T^- does not result in significantly lower charge extraction efficiencies, which is in agreement with ref 13.

CONCLUSIONS

We have studied the dynamics of electron injection from ruthenium-based dyes into mesoporous oxide films using ultrafast THz conductivity measurements. In an inert environment (air or acetonitrile), electron injection in dye−TiO_2 was found to occur with biphasic kinetics, in which the fast injection component (<150 fs) corresponds to injection from the excited dye singlet state and the slow injection component (∼10 ps) corresponds to injection from the excited triplet state of the dye. In contrast, electron injection into SnO_2 films occurs predominantly from the triplet state: although the energy difference between the dye excited state and the SnO_2 conduction band edge is larger than for the dye−TiO_2 system, the density of accepting states is much lower in SnO_2, as a result of which injection from the singlet state is no longer fast enough to compete with intersystem crossing from the singlet to the triplet state. Also, we found that electron injection is only slightly slower in the presence of an I_3^-/I^- redox couple but that injection is significantly retarded in the presence of the recently developed disulfide/thiolate (T_2/T^-) redox couple. A similar retardation of electron injection was observed for the I_3^-/I^- electrolyte in the presence of additives like Li^+ ions and TBP (4-*tert*-butyl pyridine) that are known to enhance solar cell efficiencies.[13] Especially the presence of TBP led to slower injection, which can be explained by a shift of the oxide conduction band to higher energies, leading to a decrease of the density of accepting states at the energy position of the

excited dye states. Slower electron injection is not necessarily detrimental for solar cell efficiency since injection on ultrafast time scales (<100 fs) is kinetically redundant[13] and is inherently associated with larger recombination of electrons in TiO_2 with the cationic dye or the redox couple. Positioning the conduction band at higher energies leads to slower electron injection (but still fast enough to extract the majority of photogenerated carriers) but significantly reduces recombination of electrons in TiO_2.

■ ASSOCIATED CONTENT

Supporting Information. Figure S1 showing absorption spectra of dye-sensitized TiO_2 films and Figure S2 showing the absorption spectra for the T^-/T_2 redox couple and the I^-/I_2 redox couple in acetonitrile. This material is available free of charge via the Internet at http://pubs.acs.org.

■ AUTHOR INFORMATION

Corresponding Author
*Tel.: +31 20 7547100. Fax: +31 20 7547290. E-mail: bonn@amolf.nl.

■ ACKNOWLEDGMENT

We thank Frank Lenzmann and Klaas Bakker of the Energy Center Netherlands for determining the current−voltage characteristics. This work is part of the Joint Solar Programme (JSP) of the Stichting voor Fundamenteel Onderzoek der Materie FOM, which is supported financially by Nederlandse Organisatie voor Wetenschappelijk Onderzoek (NWO). The JSP is cofinanced by gebied Chemische Wetenschappen of NWO and Stichting Shell Research.

■ REFERENCES

(1) O'Regan, B.; Gratzel, M. *Nature* **1991**, *353*, 737–740.
(2) Gratzel, M. *Nature* **2001**, *414*, 338–344.
(3) Tachibana, Y.; Moser, J. E.; Gratzel, M.; Klug, D. R.; Durrant, J. R. *J. Phys. Chem.* **1996**, *100*, 20056–20062.
(4) Asbury, J. B.; Hao, E.; Wang, Y.; Ghosh, H. N.; Lian, T. *J. Phys. Chem. B* **2001**, *105*, 4545–4557.
(5) Asbury, J. B.; Anderson, N. A.; Hao, E.; Ai, X.; Lian, T. *J. Phys. Chem. B* **2003**, *107*, 7376–7386.
(6) Tachibana, Y.; Nazeeruddin, M. K.; Grätzel, M.; Klug, D. R.; Durrant, J. R. *Chem. Phys.* **2002**, *285*, 127–132.
(7) Turner, G. M.; Beard, M. C.; Schmuttenmaer, C. A. *J. Phys. Chem. B* **2002**, *106*, 11716–11719.
(8) Abuabara, S. G.; Cady, C. W.; Baxter, J. B.; Schmuttenmaer, C. A.; Crabtree, R. H.; Brudvig, G. W.; Batista, V. S. *J. Phys. Chem. C* **2007**, *111*, 11982–11990.
(9) Huang, J.; Stockwell, D.; Boulesbaa, A.; Guo, J.; Lian, T. *J. Phys. Chem. C* **2008**, *112*, 5203–5212.
(10) McNamara, W. R.; Snoeberger, R. C.; Li, G.; Schleicher, J. M.; Cady, C. W.; Poyatos, M.; Schmuttenmaer, C. A.; Crabtree, R. H.; Brudvig, G. W.; Batista, V. S. *J. Am. Chem. Soc.* **2008**, *130*, 14329–14338.
(11) Tiwana, P.; Parkinson, P.; Johnston, M. B.; Snaith, H. J.; Herz, L. M. *J. Phys. Chem. C* **2010**, *114*, 1365–1371.
(12) Marcus, R. A. *J. Chem. Phys.* **1965**, *43*, 679–701.
(13) Haque, S. A.; Palomares, E.; Cho, B. M.; Green, A. N. M.; Hirata, N.; Klug, D. R.; Durrant, J. R. *J. Am. Chem. Soc.* **2005**, *127*, 3456–3462.
(14) Koops, S. E.; O'Regan, B. C.; Barnes, P. R. F.; Durrant, J. R. *J. Am. Chem. Soc.* **2009**, *131*, 4808–4818.
(15) Haque, S. A.; Tachibana, Y.; Willis, R. L.; Moser, J. E.; Gratzel, M.; Klug, D. R.; Durrant, J. R. *J. Phys. Chem. B* **2000**, *104*, 538–547.
(16) Wang, M.; Chamberland, N.; Breau, L.; Moser, J.-E.; Humphry-Baker, R.; Marsan, B.; Zakeeruddin, S. M.; Grätzel, M. *Nat. Chem.* **2010**, *2*, 385–389.
(17) Beard, M. C.; Turner, G. M.; Schmuttenmaer, C. A. *J. Phys. Chem. B* **2002**, *106*, 7146–7159.
(18) Jeon, T.-I.; Grischkowsky, D. *Phys. Rev. Lett.* **1997**, *78*, 1106.
(19) Pijpers, J. J. H.; Ulbricht, R.; Tielrooij, K. J.; Osherov, A.; Golan, Y.; Delerue, C.; Allan, G.; Bonn, M. *Nat. Phys.* **2009**, *5*, 811–814.
(20) Beard, M. C.; Turner, G. M.; Schmuttenmaer, C. A. *Phys. Rev. B* **2000**, *62*, 15764–15777.
(21) Hendry, E.; Koeberg, M.; O'Regan, B.; Bonn, M. *Nano Lett.* **2006**, *6*, 755–759.
(22) Hendry, E.; Wang, F.; Shan, J.; Heinz, T. F.; Bonn, M. *Phys. Rev. B* **2004**, 69.
(23) Němec, H.; Kužel, P.; Sundström, V. *Phys. Rev. B* **2009**, *79*, 115309.
(24) Hannappel, T.; Burfeindt, B.; Storck, W.; Willig, F. *J. Phys. Chem. B* **1997**, *101*, 6799–6802.
(25) Benko, G.; Kallioinen, J.; Korppi-Tommola, J. E. I.; Yartsev, A. P.; Sundstrom, V. *J. Am. Chem. Soc.* **2002**, *124*, 489–493.
(26) Enright, B.; Fitzmaurice, D. *J. Phys. Chem.* **1996**, *100*, 1027–1035.
(27) Bak, T.; Nowotny, J.; Rekas, M.; Sorrell, C. C. *Int. J. Hydrogen Energy* **2002**, *27*, 991–1022.
(28) Button, K. J.; Fonstad, C. G.; Dreybrodt, W. *Phys. Rev. B* **1971**, *4*, 4539.
(29) Hook, J. R.; Hall, H. E. *Solid State Physics*; John Wiley & Sons: Chichester, 2004.